JACS
JOURNAL OF THE AMERICAN CHEMICAL SOCIETY
Article
pubs.acs.org/JACS

# Solvent-Templated Folding of Perylene Bisimide Macrocycles into Coiled Double-String Ropes with Solvent-Sensitive Optical Signatures

Peter Spenst,[†] Ryan M. Young,[‖] Brian T. Phelan,[‖] Michel Keller,[‡] Jakub Dostál,[‡] Tobias Brixner,[‡,§] Michael R. Wasielewski,*[,‖] and Frank Würthner*[,†,§]

[†]Institut für Organische Chemie, [‡]Institut für Physikalische und Theoretische Chemie, and [§]Center for Nanosystems Chemistry, Universität Würzburg, 97074 Würzburg, Germany

[‖]Department of Chemistry, Argonne-Northwestern Solar Energy Research (ANSER) Center, Northwestern University, 2145 Sheridan Road, Evanston, Illinois 60208-3113, United States

Supporting Information

**ABSTRACT:** A series of semirigid perylene bisimide (PBI) macrocycles with varied ring size containing two to nine PBI chromophores were synthesized in a one-pot reaction and their photophysical properties characterized by fluorescence, steady-state, and transient absorption spectroscopy as well as femtosecond stimulated Raman spectroscopy. These macrocycles show solvent-dependent conformational equilibria and excited-state properties. In dichloromethane, the macrocycles prevail in wide-stretched conformations and upon photoexcitation exhibit symmetry-breaking charge separation followed by charge recombination to triplet states, which photosensitize singlet oxygen formation. In contrast, in aromatic solvents folding of the macrocycles with a distinct odd−even effect regarding the number of PBI chromophore units was observed in steady-state and time-resolved absorption and fluorescence spectroscopy as well as femtosecond stimulated Raman spectroscopy. These distinctive optical properties are attributable to the folding of the even-membered macrocycles into exciton-vibrational coupled dimer pairs in aromatic solvents. Studies in a variety of aromatic solvents indicate that these solvents embed between PBI dimer pairs and accordingly template the folding of even-membered PBI macrocycles into ropelike folded conformations that give rise to solvent-specific exciton-vibrational couplings in UV−vis absorption spectra. As a consequence of the embedding of solvent molecules in the coiled double-string rope architecture, highly solvent specific intensity ratios are observed for the two lowest-energy exciton-vibrational bands, enabling assignment of the respective solvent simply based on the absorption spectra measured for the tetramer macrocycle.

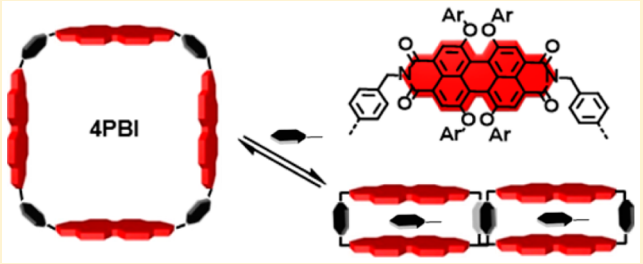


## INTRODUCTION

The organization of π-conjugated molecules into defined structures plays a unique role in chemistry and biology to create specific functions. Outstanding examples in nature are the self-organization of DNA into double helices[1] or the fixation of chlorophyll and bacteriochlorophyll arrays into macrocyclic structures in light-harvesting systems of purple bacteria.[2] Whereas in nature a sophisticated matrix of proteins and numerous noncovalent interactions force the dye subunits into defined arrangements, it is of interest to explore simpler approaches to direct the dye molecules to a desired organization in a specific environment.[3] Such a control of molecular structure is crucial also for artificial counterparts, knowing that the position of the dyes to each other defines the photophysical processes that occur in the composite because small changes can lead to quite different electronic interactions.[4]

Perylene bisimide (PBI) dyes are well-suited for such studies since their conformation and photophysical properties are easy to tune by substitution in the imide or bay positions.[5] Thus, multichromophoric PBI systems could be used to study electronic interactions in defined self-assembled or covalently tethered ensembles.[5,6] Indeed, covalent linkage of PBI chromophores has been used quite extensively for the preorganization of dyes to give arrangements with specific photophysical properties.[7] Furthermore, in a smaller number of studies the transition between different conformations has been demonstrated by changing solvent polarity, inducing folding of backbone-tethered PBI oligomers.[8] In these foldamers[9] with different backbone lengths, π−π interactions between the dyes were used to create highly ordered assemblies with defined geometry that were explored by optical spectroscopy. Likewise, rigid PBI macrocycles[10] and a variety of cyclophanes[11,12] have previously been reported.[13] These studies include **2PBI** (Figure 1), which showed a variety of exciting and in part

**Received:** November 20, 2016
**Published:** January 12, 2017





DOI: 10.1021/jacs.6b11973
J. Am. Chem. Soc. 2017, 139, 2014−2021

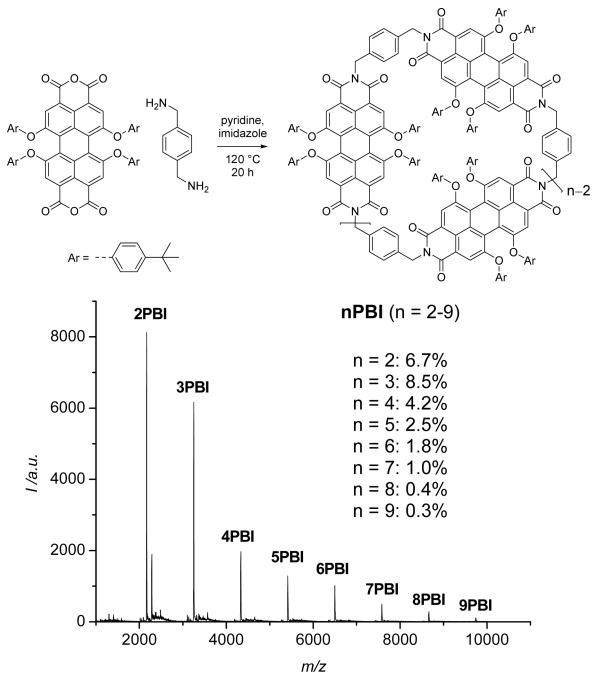


**Figure 1.** Synthesis of PBI macrocycles ***n*PBI** and MALDI-TOF spectrum of the crude product mixture prior to separation of the individual macrocycles (pos. mode, DCTB in chloroform 1:1).

unprecedented properties: (a) ability to form strong host–guest complexes with binding constants up to $\sim 10^5$ $M^{-1}$ with large aromatic $\pi$-systems such as perylene;[12a] (b) solvent- and guest-dependent excited-state relaxation with intense fluorescence in toluene and in the presence of electron-poor guest molecules versus strongly quenched emission due to photoinduced electron transfer in the presence of electron-rich guests or due to symmetry-breaking charge separation (SB-CS)[14] and subsequent triplet-state population in dichloromethane.[12b] These features could be related to a well-shaped rather rigid cavity that enables the encapsulation of aromatic solvents or larger aromatic $\pi$-systems that modulate the interaction of the two PBI chromophores in the photoexcited state.

Herein we present our subsequent study on the homologous oligomer series derived from **2PBI**, i.e., PBI macrocycles ***n*PBI** ($n$ = 3–9) where numerous PBI chromophores ($n$) are covalently linked through *para*-xylylene bridges. As we will show, a folding of the macrocycles can be initiated with a significant odd–even effect regarding the number of PBI chromophores in aromatic solvents like toluene. The photophysical properties of folded (in toluene) and unfolded (in dichloromethane) PBI macrocycles have been studied by fluorescence, steady-state and transient absorption (TA) spectroscopy, and femtosecond stimulated Raman spectroscopy (FSRS) revealing a folding-modulated excited-state behavior. Our results are rationalized by a templating effect of aromatic solvents that direct a conformational change of the even-membered macrocycles ($n$ = 4, 6, 8) from a wide-stretched conformation to a coiled double-string conformation. To the best of our knowledge, such conformational changes in macrocyclic structures and accompanying changes in photophysical properties through solvent-specific intramolecular dye–dye interactions are to date unprecedented.

## RESULTS AND DISCUSSION

**Synthesis.** PBI macrocycles ***n*PBI** ($n$ = 2–9) were synthesized by imidization of 1,6,7,12-tetrakis-4-*tert*-butylphenoxy-perylene-3,4:9,10-tetracarboxylic acid bisanhydride with 1 equiv of *para*-xylylenediamine in imidazole and pyridine in a one-pot reaction at 120 °C under inert conditions. MALDI-TOF mass spectrum of the crude product mixture clearly showed the formation of macrocycles with different ring sizes starting with the dimer **2PBI**, containing two PBI units, to the nonamer **9PBI**, with nine covalently linked PBI chromophores (Figure 1). Furthermore, we note the presence of impurities arising from open-chain oligomers with higher mass than the respective macrocycles. The purification and separation of the macrocycles were achieved by column chromatography (silica gel, $CH_2Cl_2$/MeOH 9:1), which removes insoluble polymeric and oligomeric side products and also separates the cyclic dimer **2PBI** from the larger macrocycles, followed by several recycling GPC (gel permeation chromatography) runs using chloroform as an eluent. Thus, pure ***n*PBI** macrocycles ($n$ = 2–9) were isolated in yields of 6.7, 8.5, 4.2, 2.5, 1.8, 1.0, 0.4, and 0.3%, respectively. The relatively low total yield of all macrocycles (~25%) and the decrease of the yield with increasing ring size (trimer to nonamer) is due to the fact that the macrocycles are formed by intramolecular ring closure of the respective open-chain intermediates, which becomes less favored with increasing ring size.

Despite the low isolated yields, the individual macrocycles could be obtained as pure products and satisfactorily characterized by mass spectrometry, $^1$H and $^{13}$C NMR, and optical spectroscopy. The $^1$H NMR spectra of macrocycles ***n*PBI** ($n$ = 2–9) in chloroform show one set of signals confirming the high symmetry of the molecules (Figure S1). In comparison to monomeric reference compound **1PBI** bearing benzyl groups in the imide positions of the PBI, a slight upfield shift of the PBI core protons occurs, which is strongest for **2PBI** due to close contact of the chromophores and gets smaller with increasing ring size and angle between the dyes. This indicates that with increasing ring size the contact between the PBI chromophores is reduced in chloroform so that the chromophores in the larger cycles behave more like the monomeric **1PBI**.

**Steady-State UV–Vis Absorption and Fluorescence Properties.** The optical properties of dimer **2PBI** have been reported previously and thus will not be discussed here in detail.[12] However, the relevant data for **2PBI** are given to provide a complete picture of this series of macrocycles. To start our investigation we utilized dichloromethane as a solvent that is known for its excellent solvation properties for PBI dyes.[15] The steady-state absorption spectra ($c = 5 \times 10^{-6}$ M) of the macrocycles in this solvent display the typical band shape of monomeric PBIs (Figure S2). While the $S_0$–$S_2$ transition provides only a broad signal between 400 and 500 nm, a characteristic vibronic fine structure can be observed for the $S_0$–$S_1$ transition with maxima at around 580 ($A_{0-0}$) and vibronic progressions at 540 nm ($A_{0-1}$). The corresponding fluorescence spectra are the mirror images of the $S_0$–$S_1$ absorption spectra with maxima at 620 nm. These results suggest that in dichloromethane all macrocycles ($n > 2$) prevail in wide-stretched conformations where PBI–PBI interactions are absent. In contrast, upon changing the solvent to aromatic toluene some of the macrocycles reveal remarkable changes of their spectra. While the cycles with odd numbers of PBI units


DOI: 10.1021/jacs.6b11973
J. Am. Chem. Soc. 2017, 139, 2014–2021

still show the typical monomer-type band shape (Figure 2a), a strong increase of the 0−1 vibronic transition band for the even

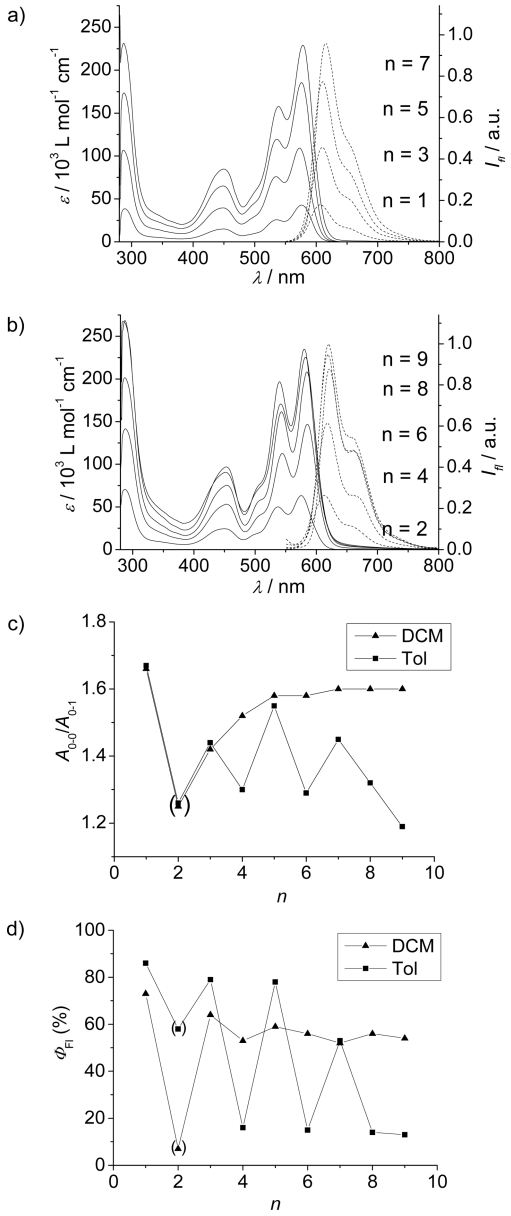


**Figure 2.** (a, b) UV−vis (solid line) and fluorescence spectra (dashed line) of ***n*PBI** ($n$ = 1−9) in toluene ($5 \times 10^{-6}$ M); fluorescence spectra are normalized to the corresponding maximum in the absorption (298 K). Plots of the $A_{0-0}/A_{0-1}$ ratio (c) and fluorescence quantum yields $\Phi_{Fl}$ (d) of ***n*PBI** vs the number of chromophores $n$ in dichloromethane (▲) and toluene (■); the connecting lines serve the purpose of visualization and do not imply any fitting.

cycles is observed, indicating an increased interaction, i.e., exciton coupling between the molecules (Figure 2b).[16]

To elucidate whether these spectral changes of the even-numbered macrocycles in the absorption bands originate from intermolecular or intramolecular couplings, i.e., PBI aggregation by self-assembly or folding, concentration-dependent UV−vis absorption studies of **4PBI** were performed in toluene ($2.5 \times 10^{-5}$−$3.5 \times 10^{-7}$ M, Figure S3). With dilution of the sample no changes in the spectra occur, which excludes the formation of self-assembled larger aggregates of the macrocycles and corroborates intramolecular folding in toluene.

The $A_{0-0}/A_{0-1}$ ratio in the UV−vis absorption spectra has been often used to distinguish between uncoupled monomer-like PBIs and those influenced by exciton coupling among each other.[16] For the given series, values of ∼1.60 are observed for ***n*PBI** with $n$ = 5−9 in dichloromethane that are very close to that of the reference monomer **1PBI** ($A_{0-0}/A_{0-1}$ (**1PBI**) = 1.66). With decreasing ring size, the $A_{0-0}/A_{0-1}$ ratio is reduced to 1.52, 1.42, and 1.25 for **4PBI**, **3PBI** and **2PBI**, respectively.[16d] In toluene, the $A_{0-0}/A_{0-1}$ ratio for even-numbered **4PBI**, **6PBI**, and **8PBI** is markedly reduced to ∼1.3 indicating a significant interchromophoric coupling within these cycles in their folded state. For the odd-numbered cycles, the $A_{0-0}/A_{0-1}$ ratio diminishes from 1.55 to 1.45 and 1.19 for **5PBI**, **7PBI**, and **9PBI** suggesting partial folding with increasing ring size (all data are summarized in Table 1 and

**Table 1. Characteristic Optical Spectroscopic Data of *n*PBI ($n$ = 1−9) in Dichloromethane and Toluene (298 K)**

| $n$ | $A_{0-0}/A_{0-1}$ ($CH_2Cl_2$) | $A_{0-0}/A_{0-1}$ (Tol) | $\Phi_{Fl}$ ($CH_2Cl_2$) | $\Phi_{Fl}$ (Tol) |
|---|---|---|---|---|
| 1 | 1.66 | 1.67 | 0.73 | 0.86 |
| 2 | 1.25 | 1.26 | 0.07 | 0.58 |
| 3 | 1.42 | 1.44 | 0.64 | 0.79 |
| 4 | 1.52 | 1.30 | 0.53 | 0.16 |
| 5 | 1.58 | 1.55 | 0.59 | 0.78 |
| 6 | 1.58 | 1.29 | 0.56 | 0.15 |
| 7 | 1.60 | 1.45 | 0.52 | 0.53 |
| 8 | 1.60 | 1.32 | 0.56 | 0.14 |
| 9 | 1.60 | 1.19 | 0.54 | 0.13 |

graphically visualized in Figure 2c). Notably, for the two smallest and most rigid macrocycles, **2PBI** and **3PBI**, identical $A_{0-0}/A_{0-1}$ ratios are observed in dichloromethane and toluene which suggests the presence of similar conformations in both solvents.

Concomitantly, with the changes observed for the $A_{0-0}/A_{0-1}$ ratio in UV−vis absorption spectra, the fluorescence is significantly quenched in toluene for even-membered macrocycles **4PBI**, **6PBI**, and **8PBI** with quantum yields of only $\Phi_{Fl}$ ≈ 15% compared to that of monomer reference **1PBI** ($\Phi_{Fl}$ = 86%), indicating the presence of additional nonradiative decay channels due to the interacting PBI units. For the odd-numbered macrocycles, the fluorescence quantum yields remain high for cycles **3PBI**, **5PBI**, and **7PBI** and only decreases significantly for the largest **9PBI** to 13%.

In dichloromethane, with the exception of **2PBI**, fluorescence quantum yields are only a little affected and remain high for the whole series ($\Phi_{Fl}$ = 52−64%). Accordingly, the changes in the fluorescence quantum yields follow exactly the same trend as that observed for the $A_{0-0}/A_{0-1}$ ratios, supporting the presence of folded species for even-membered macrocycles and increasing amounts of folded species for odd-membered macrocycles with increasing ring size (Figure 2d).

**Solvent Effects.** To clarify the origin of the peculiar properties of PBI macrocycles in toluene, we further analyzed the absorption properties of **4PBI** in a series of nonaromatic solvents (acetone, THF, $CH_2Cl_2$, $CHCl_3$, $Et_2O$, dioxane, and $CCl_4$, with $\varepsilon_r$ = 20.7, 9.10, 7.60, 4.81, 4.30, 2.25, and 2.24, respectively). For all of these solvents, characteristic monomer-like bandshapes and $A_{0-0}/A_{0-1}$ ratios were observed (Figure S4a), corroborating the presence of unfolded wide-stretched


DOI: 10.1021/jacs.6b11973
J. Am. Chem. Soc. 2017, 139, 2014−2021

conformations. Thus, solvent polarity can be excluded as the driving force for the folding process.

Since the folding so far was only observed in toluene, other aromatic solvents were next examined by UV−vis absorption spectroscopy. By comparison of the $A_{0-0}/A_{0-1}$ ratios to the previously discussed values of the corresponding $CH_2Cl_2$ solutions in which the macrocycles are in their unfolded state, the degree of folding in the individual aromatic solvent can be monitored (Figures 3 and S4b; Table S1). For

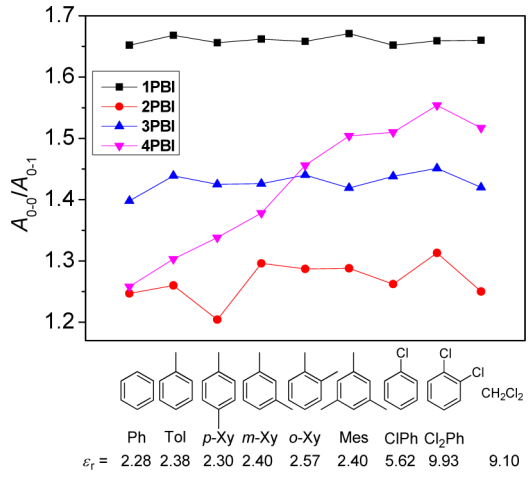


**Figure 3.** Plots of the $A_{0-0}/A_{0-1}$ ratios in different aromatic solvents and $CH_2Cl_2$ for **1PBI** (black), **2PBI** (red), **3PBI** (blue), and **4PBI** (purple) at 298 K.

monomeric reference **1PBI**, a value of ∼1.66 was found for all the applied solvents confirming that no intermolecular interactions between the solvent molecules and the given chromophore influence the band shape (Figure 3, black line). In dimer **2PBI** (red line) and trimer **3PBI** (blue line), lower values of ∼1.3 (dimer) and ∼1.4 (trimer) are observed. The values are, however, rather independent of the respectively solvent which suggests solvent-independent conformations, i.e., rigid scaffolds.

In contrast, the $A_{0-0}/A_{0-1}$ ratios for **4PBI** differ strongly depending on the type of aromatic solvents from 1.26 in benzene to 1.55 in *ortho*-dichlorobenzene (purple line). This indicates a successive shift of the equilibrium toward the folded state in the order of $Cl_2Ph$ < ClPh < Mes < *o*-Xy < *m*-Xy < *p*-Xy < Tol < Ph (Figure 3). Similar trends can be observed for the folding of the larger macrocycles **6PBI**, **8PBI**, and **9PBI**; however, the order of the solvent that promotes the folding differs (Figure S4b). Clearly, also in this solvent series no relationship between folding tendency and solvent polarity can be deduced. Instead, these experiments indicate that the position and number of the methyl or chlorine groups in the aromatic solvent molecules plays a role for the conformational preference and PBI−PBI interactions of the macrocycles. The most obvious rationale for such an effect is that the solvent molecules template the particular folded conformation of these macrocycles.

It is indeed particularly impressive that the $A_{0-0}/A_{0-1}$ ratio for **4PBI** (and similarly other odd-numbered ***n*PBIs**, see Figure S4b) is able to distinguish the utilized aromatic solvents, giving specific values of 1.26 (Ph), 1.30 (Tol), 1.34 (*p*-Xy), 1.38 (*m*-Xy), 1.46 (*o*-Xy), 1.50 (Mes), 1.51 (ClPh), and 1.55 ($Cl_2Ph$). Accordingly, **4PBI** can be utilized as a molecular probe for the determination of the given aromatic solvent.

**Conformational Preferences.** In our previous investigations for **2PBI** we could demonstrate that this rigid cyclophane acts as a good host molecule in chloroform which can bind various planar aromatic guest molecules with appreciable binding constants.[12] For the larger macrocycles investigated here such binding properties are absent which can be attributed to a lack of preorganization, i.e., the prevalence of wide-stretched conformations in the majority of solvents.

This conformational preference obviously changes for the even-numbered macrocycles in aromatic solvents that exert a template effect to shift the conformational equilibrium toward conformations with pronounced PBI−PBI interactions. The fact that identical $A_{0-0}/A_{0-1}$ ratios are observed for **2PBI** and **4PBI** in benzene (Figure 3) indeed corroborates the perception that similar PBI−PBI contacts are given for **2PBI** and folded **4PBI** as suggested in Figure 4. On the basis of our in-depth

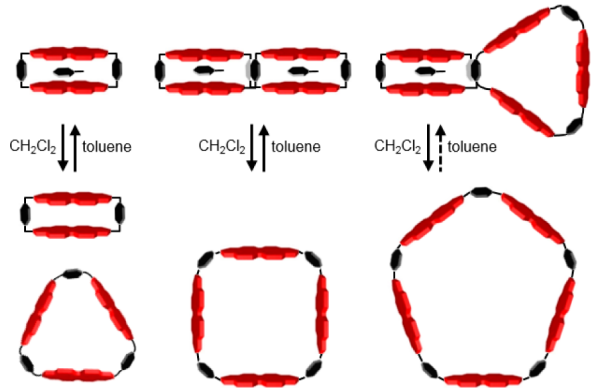


**Figure 4.** Schematic comparison between solvent-independent rigid conformations of **2PBI** and **3PBI** versus solvent-dependent conformational changes of PBI macrocycles **4PBI** and **5PBI**.

studies for **2PBI**, it is accordingly reasonable to assume that one or more aromatic solvents fill up the space between a PBI dye pair also for **4PBI** as illustrated in Figure 4. Thus, under the template effect of the solvent molecules the PBI oligomer chain of even-membered macrocycles, as exemplified in Figure 4 for **4PBI**, coils into a double-string rope leading to the observed spectral features. Thereby, subtle steric differences of the respectively incorporated solvent molecules modulate the $A_{0-0}/A_{0-1}$ ratio in a rather specific way.

To get a better understanding of the folded structures, NMR spectroscopy is the typical method of choice. For the given macrocycles, however, solubility is too limited (<0.1 mM) in aromatic solvents where the templating effect is observed. Furthermore, tetraphenoxy-substituted PBIs show broken-symmetry asymmetric structures in all single crystals as well as at low temperatures in solution, giving raise to complex NMR patterns.[17] For these reasons, further insights were taken from molecular modeling studies of **4PBI** using force field calculations (Figure 5). The geometry-optimized structure corroborates the presence of a pleated geometry consisting of two PBI pairs whose interchromophore distance of around 6.8 Å appears ideally suited to embed aromatic solvent molecules. Because of the two crossing xylene linkers, the PBI dyes have a twisted arrangement of 15° to each other that directs two bay substituents of each PBI molecule into the cavity of the folded PBI dimers. This might explain why the folded macrocycles do


DOI: 10.1021/jacs.6b11973
J. Am. Chem. Soc. 2017, 139, 2014−2021

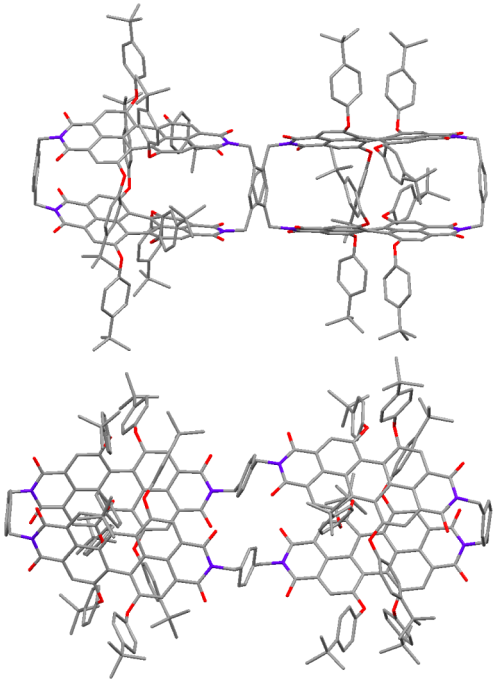

**Figure 5.** Geometry-optimized structure of the folded **4PBI** in side view (top) and top view (bottom) obtained by force field optimization; Maestro 9.3, MacroModel 9.8, MM2*.

not behave in all properties like the rigid **2PBI** with its more rigid cofacial arrangement of the chromophores and why rather similar solvents afford distinguishable optical signals for **4PBI**. Thus, it is the conformationally rather flexible phenoxy-substitutents[18] whose arrangement is governed by the respective embedded solvent molecules.

Assuming that this structural motif can also be adapted to **6PBI** and **8PBI**, the observed similar optical properties of the even-numbered macrocycles can be explained, although with increasing flexibility other folded patterns might be possible as well. It is clear that the odd-numbered cycles cannot form such pairs of dimers including all the chromophore units and that the smaller trimer forms a rather rigid triangular structure (Figure 4). For **5PBI**, the folding equilibrium appears to be strongly biased toward the wide-stretched pentagon conformation depicted in Figure 4 even in toluene according to the $A_{0-0}/A_{0-1}$ ratio and the fluorescence quantum yields (Figure 2c,d). With the higher flexibility of the larger macrocycles, the equilibrium shifts toward more folded motifs in aromatic solvents. Thus, in the limit of our study, for **9PBI** both $A_{0-0}/A_{0-1}$ ratio and fluorescence quantum yield suggest the presence of a mostly pleated structure in toluene that might consist of three pairs of PBIs and one triangular arrangement.

**Solvent-Dependent Folding Equilibria.** While a binding of aromatic molecules could not be observed by conventional titration experiments for macrocycles larger than **2PBI**, the transition between unfolded and folded conformations could be easily monitored by UV−vis absorption spectroscopy of the tetrameric cycle **4PBI** in different mixtures of dichloromethane and toluene (Figure S5). From these absorption spectra, it is obvious that more than 70% toluene is needed to induce the folding process which explains the failure of **4PBI** to give host−guest complexes with aromatic guest molecules in well-solvating solvents such as chloroform as observed for the rigid and properly preorganized **2PBI**.[12a] Nevertheless, the successive decrease of the $A_{0-0}/A_{0-1}$ ratio at higher toluene contents allows us to estimate the free energy for the folding process in toluene according to the method of Moore and Ray (Figure 6).[19] For this determination two assumptions have to

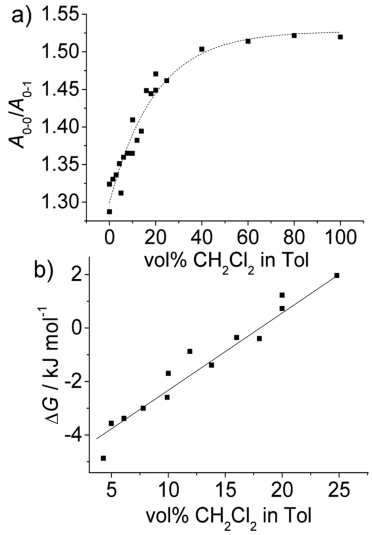


**Figure 6.** (a) Changes in the $A_{0-0}/A_{0-1}$ ratio of **4PBI** in $CH_2Cl_2$/toluene mixtures at 298 K and (b) plot of the $\Delta G$ values for the folding process derived from the spectral development at the 0−0 transition band. The solid line represents the fitting curve from linear regression according to eq 4.

be made: (1) The extinction coefficient $\varepsilon_U$ in $CH_2Cl_2$ solution corresponds to the entirely unfolded state. 2) The extinction coefficient $\varepsilon_F$ found in toluene is related to the folded state.

From there on, the mole fraction $\alpha_U$ of chromophores in the unfolded state can be estimated for all solvent mixtures using

$$\alpha_U = \frac{\varepsilon_F - \varepsilon_{obs}}{\varepsilon_F - \varepsilon_U} \quad (1)$$

where $\varepsilon_{obs}$ is the extinction value for the individual solvent mixture at the 0−1 or 0−0 transition band. The equilibrium constant $K_{eq}$ and the Gibbs free energy changes $\Delta G$ for each solvent composition can then be calculated according to

$$K_{eq} = \frac{c_F}{c_U} = \frac{1 - \alpha_U}{\alpha_U} \quad (2)$$

$$\Delta G = -RT \ln K_{eq} \quad (3)$$

where $c_F$ and $c_U$ are the concentrations of the folded and unfolded species, respectively.

Analogous to the solvent denaturation of proteins and peptide secondary structures, the free energy change between both conformations is assumed to behave linearly with the solvent composition.[20] This enables the estimation of the Gibbs free energy in pure toluene by extrapolation of the fitting line of the $A_{0-0}$ transition band to −5.3 ± 0.2 kJ/mol with a slope of $m$ = 292 ± 13 J/mol (Figure 6) according to

$$\Delta G = \Delta G(\text{Tol}) + m[CH_2Cl_2] \quad (4)$$

The detailed thermodynamic data obtained by this analysis are given in Table S2.

**Femtosecond Stimulated Raman Spectroscopy.** FSRS is a powerful tool for structural characterization, especially of fluorescent systems. FSRS measurements were performed on


DOI: 10.1021/jacs.6b11973
J. Am. Chem. Soc. 2017, 139, 2014−2021

***n*PBI** ($n$ = 1−5) using a preresonant Raman pump centered at 610 nm (0.6 $\mu$J/pulse) to probe the steady-state geometry of the PBI macrocycles. No actinic pump pulse was used, so the spectra are the ground-state Raman spectra of ***n*PBI** ($n$ = 1−5). The characteristic in-plane C═C stretching modes of the excited PBI core at 1360, 1395, 1456, 1548, and 1590 cm$^{-1}$ were observed in dichloromethane (Figure 7).[21] From these

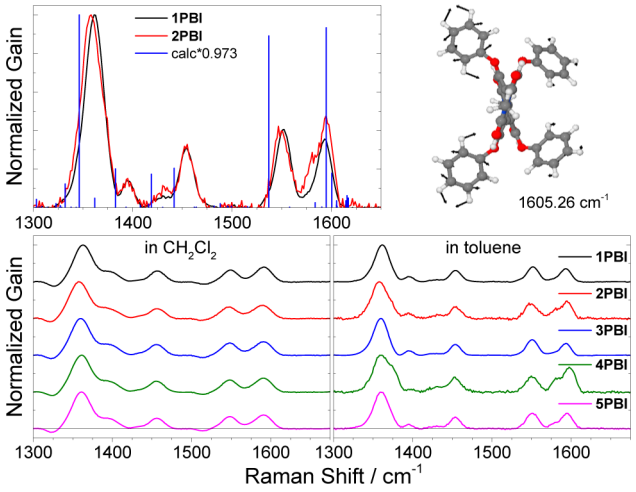


**Figure 7.** Normalized femtosecond stimulated Raman spectra of **1PBI** and **2PBI** in toluene with calculated Raman frequencies (scaled by 0.973) for **1PBI** overlaid (top-left) and **1PBI** to **5PBI** in dichloromethane (bottom-left) and toluene (bottom-right). Example mode involving phenoxy-subsitituents (top-right). $\lambda_{RP}$ = 610 nm, 0.6 $\mu$J/pulse, 298 K.

studies it is obvious that the relative intensities of the Raman bands of the macrocycles do not change compared to those of monomeric reference **1PBI** in dichloromethane, indicating that there is only subtle interchromophoric vibrational coupling within the macrocycles, even for **2PBI**. In toluene, however, the relative ratio of the 1550 and 1594 cm$^{-1}$ bands, $I_{1550}/I_{1594}$, show a similar odd−even trend as observed in other techniques (Figure 7). **1PBI** and **3PBI** have $I_{1550}/I_{1594} > 1$, **2PBI** and **4PBI** have $I_{1550}/I_{1594} < 1$, and **5PBI** has $I_{1550}/I_{1594} \approx 1$. Since the FSRS spectra in dichloromethane indicate that $I_{1550}/I_{1594}$ is insensitive to the exciton coupling that leads to the changes in $A_{0-0}/A_{0-1}$, the Raman frequencies were calculated (DFT B3LYP, 6-31G*) for **1PBI** to provide insight into the changes in $I_{1550}/I_{1594}$. The normal-mode analysis revealed several low-intensity modes near 1600 cm$^{-1}$ (scaled by 0.973) involving C═C stretches on the phenoxy-substituents (Figures 7 and S17; Table S3), indicating that changes in $I_{1550}/I_{1594}$ may result from interactions involving the phenoxy-substituents and neighboring PBI cores or embedded solvent molecules. Thus, $I_{1550}/I_{1594}$ is indicative of the folded or wide-stretched geometries present in the PBI macrocycles. Furthermore, **5PBI** has $I_{1550}/I_{1594}$ in between that of **1/3PBI** and **2/4PBI**, further supporting that the larger odd macrocycles fold to form a combination of dimer and trimer units as suggested in Figure 4 for **5PBI**.

There is one important issue to keep in mind when discussing UV−vis absorption, FSRS, and fluorescence spectroscopy data. The absorption and (steady-state) FSRS data result from optical excitations of molecules in the ground state that exist in their thermally equilibrated conformational manifold. Upon excitation these molecules are promoted into their excited states that are, in contrast, not equilibrated. Furthermore, at low-to-moderate light intensities only one molecule in the macrocycle is optically excited while the others prevail in the ground state. Such excited macrocycles may exhibit various relaxation pathways into energetically more favorable geometries and/or electronically more stable configurations, e.g., excimers, charge transfer states, and so on.[22] The respective states will finally determine the relaxation path back to the ground state via radiative and nonradiative pathways. According to our data from steady-state fluorescence spectroscopy, we can recognize a quite uniform behavior for all cycles in dichloromethane except for **2PBI**.

The exceptional behavior of the latter could be related to an unusually fast SB-CS in our earlier studies and will accordingly not be discussed here.[12b] Instead, we utilize time-resolved spectroscopy to gain insights into the different relaxation pathways in dichloromethane and toluene for the larger macrocycles.

**Excited-State Properties.** To elucidate the excited-state dynamics of the macrocycles, we performed femtosecond (fs) and nanosecond (ns) transient absorption (TA) spectroscopy. Due to a low solubility of the larger macrocycles in toluene, we restricted these studies on **3PBI**, **4PBI**, and **5PBI**. In dichloromethane, all of these macrocycles showed similar dynamics after photoexcitation at 580 nm (Figures 8, S8, S11,

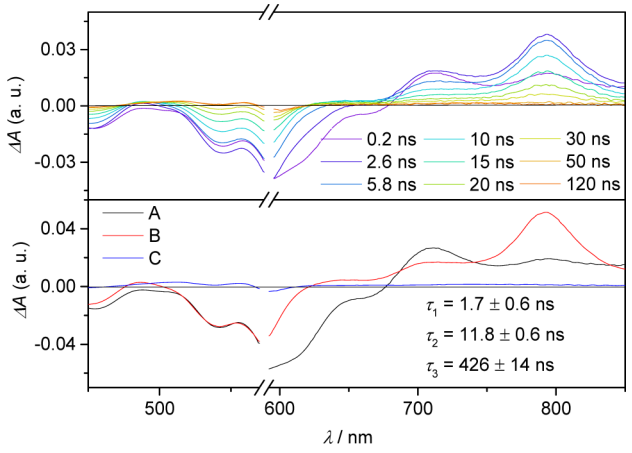


**Figure 8.** Nanosecond transient absorption spectra (top) of **4PBI** in dichloromethane showing excited-state dynamics after photoexcitation; species-associated spectra plots (bottom) reconstructed from global fits to the sequential A → B → C → ground-state model, where A is the singlet excited state $S_1$, B is the charge-separated state SB-CS, and C is the PBI triplet $T_1$ ($\lambda_{ex}$ = 580 nm, 1.0 $\mu$J/pulse, 298 K).

and S14) with the ground-state bleach (GSB) at 458, 543, and 585 nm, stimulated emission (SE) at 610 and 658 nm, and the excited-state absorption (ESA) at 707, 952, and 1031 nm, typical of tetraphenoxy-PBIs.[10c,12b] After 3.1 ± 0.2 ns, **3PBI** reaches a new transient species that can be identified as the SB-CS similar to those of the previously published **2PBI** and other PBI macrocycles.[10c,12b] In this state, new bands for the PBI radical anion and cation are present at 797, 993, and 1100 nm ($PBI^{-\bullet}$) and at 486, 628, and 1220 nm ($PBI^{+\bullet}$).[10c]

The much slower charge separation in **3PBI** (3.1 ± 0.2 ns) compared to that in **2PBI** (161 ± 4 ps) is a clear indication that this process occurs through space between the PBI cores and not through bonds because the PBI dyes are spatially further apart from each other in **3PBI** than in **2PBI**. In **4PBI** and **5PBI**,


DOI: 10.1021/jacs.6b11973
J. Am. Chem. Soc. 2017, 139, 2014−2021

the charge separation occurs with 1.71 ± 0.06 and 2.3 ± 0.9 ns, faster than in **3PBI** (Figures S11 and S14), which can be explained in terms of a higher flexibility of the larger cycles allowing the PBI molecules to approach each other in contrast to the rather rigid **3PBI**. However, the charge separation is still much slower than in the conformationally fixed **2PBI**, which suggests that **4PBI** and **5PBI** also prevail in wide-stretched conformations both in the ground and excited states in dichloromethane.

The charges then recombine to a significant fraction to the PBI triplet state in 14.5 ± 0.6, 11.8 ± 0.6, and 12.7 ± 0.6 ns for **3PBI**, **4PBI**, and **5PBI** with a PBI triplet lifetime of 560 ± 18, 426 ± 14, and 403 ± 41 ns in an air-saturated solution (Figures S9, S12, and S15). The relatively short lifetimes of the triplet state can be explained by an energy transfer to molecular oxygen, generating singlet oxygen.[12b] With this, the quantum yield of triplet formation can be estimated through the measurement of singlet oxygen emission at 1270 nm with methylene blue as literature-known reference ($\Phi_\Delta$ = 0.57 in $CH_2Cl_2$).[23] Thereby, a quantum yield of ~20% was observed for **3PBI**, **4PBI**, and **5PBI**.

By switching the solvent to toluene, the symmetry-breaking charge separation becomes energetically unfavored, as elucidated in detail for **2PBI**;[12b] hence, the triplet pathway is prevented. Now, the radiative pathway prevails after photoexcitation explaining the higher fluorescence quantum yields (see Table 1) for the odd-numbered **3PBI** and **5PBI** in toluene (Figures S10 and S16). The excited state of even-numbered **4PBI** (Figure 9) decays with 3.8 ± 0.6 ns, much faster than that

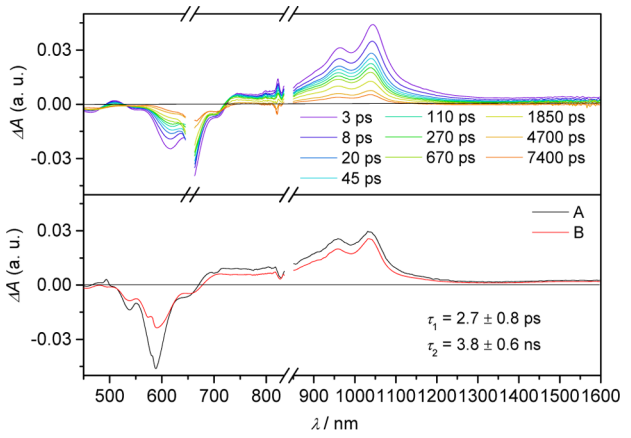


**Figure 9.** Femtosecond transient absorption spectra (top) of **4PBI** in toluene showing the excited-state dynamics after photoexcitation; species-associated spectra (bottom) reconstructed from global fits to the sequential A → B → ground state model, where A and B are $^1$*PBI ($\lambda_{ex}$ = 580 nm, 1.0 $\mu$J/pulse, 298 K).

of the odd-numbered ones (6.6 ± 0.9, 6.4 ± 0.6 ns). Furthermore, a fast decay of 2.4 ± 0.5, 2.7 ± 0.8, and 1.7 ± 0.2 ps was observed for **3PBI**, **4PBI**, and **5PBI**, respectively, which can be attributed to solvent and structural rearrangement.[18] In accordance with these results, for none of these macrocycles could an emission signal from singlet oxygen be detected in toluene.

Since our analysis which is based on species-associated spectra suggests that the excited state of **4PBI** decays directly back to the ground state without passing through any other long-living states such as an excimer,[24] nonradiative internal conversion appears to be the most reasonable explanation for the pronounced fluorescence quenching in the folded conformation of this even-numbered macrocycle. If so, then an increased vibrational coupling between the chromophores, possibly mediated by the embedded solvent or phenoxy substituents, appears as the most likely reason.

## CONCLUSIONS

In this work, a new series of PBI macrocycles with varied ring size from dimer to nonamer has been reported and their folding behavior elucidated in great detail by fluorescence, steady-state, and transient absorption spectroscopy as well as femtosecond stimulated Raman spectroscopy. For these macrocycles, a unique odd−even effect regarding the ring size could be established. The even-numbered macrocycles undergo intramolecular folding under the templating effect of aromatic solvents with concomitant fluorescence quenching to quantum yields as low as 14% and a pronounced exciton-vibrational coupling in the UV−vis absorption spectra. In contrast, the macrocycles with odd number of chromophores still show the characteristic spectral features of monomeric reference **1PBI** and converge to the folded cycles only for the largest and most flexible **9PBI**.

Transient absorption spectroscopy revealed symmetry-breaking charge separation and triplet formation for all investigated macrocycles in dichloromethane, while an accelerated internal conversion through solvent-templated folding was observed for even-numbered macrocycles in toluene. Intensity changes of the Raman frequency at 1594 cm$^{-1}$ in the excited PBI are attributed to changes in the environment of the phenoxy-substituents in the folded or wide-stretched conformations. The spectral features were supported by molecular modeling for **4PBI** showing folding to pairs of dimers that explains the unprecedented odd-even effect in the conformational and photophysical properties in the given series of macrocycles.

The solvent-templated folding of large macrocycles (with molecular masses reaching close to 10 kDa) into double-string rope architectures illustrates an interesting new avenue in the field of foldamer research. Similar to natural biomacromolecules, where function is encoded in the proper conformation, even-membered PBI macrocycles change their properties (absorption, fluorescence) with a change of conformation. Because the conformational change is here directed by embedded aromatic solvent molecules, these PBI macrocycles can be utilized as highly sensitive molecular probes to distinguish very similar solvents like *ortho-*, *meta-*, and *para-*xylene based on the intensity ratio of the exciton-vibrational transitions in simple UV−vis absorption spectra.

## ASSOCIATED CONTENT

### Supporting Information

The Supporting Information is available free of charge on the ACS Publications website at DOI: 10.1021/jacs.6b11973.

Experimental details, including synthesis, NMR, UV−vis, fs/ns TA, FSRS (PDF)

## AUTHOR INFORMATION

### Corresponding Authors

*m-wasielewski@northwestern.edu

*wuerthner@chemie.uni-wuerzburg.de

### ORCID

Brian T. Phelan: 0000-0002-5849-0319

Tobias Brixner: 0000-0002-6529-704X



DOI: 10.1021/jacs.6b11973
J. Am. Chem. Soc. 2017, 139, 2014−2021

Michael R. Wasielewski: 0000-0003-2920-5440
Frank Würthner: 0000-0001-7245-0471

### Notes

The authors declare no competing financial interest.

## ■ ACKNOWLEDGMENTS

This work has been supported by the DFG in the framework of the Research Unit FOR 1809 (T.B. and F.W.) at the Universität Würzburg and by the Chemical Sciences, Geosciences, and Biosciences Division, Office of Basic Energy Sciences, U.S. Department of Energy under grant no. DE-FG02-99ER14999 (M.R.W.) at Northwestern University.

## ■ REFERENCES

(1) Watson, J. D.; Crick, F. H. C. *Nature* **1953**, *171*, 737.
(2) (a) McDermott, G.; Prince, S. M.; Freer, A. A.; Hawthornthwaite-Lawless, A. M.; Papiz, M. Z.; Cogdell, R. J.; Isaacs, N. W. *Nature* **1995**, *374*, 517. (b) Koepke, J.; Hu, X.; Muenke, C.; Schulten, K.; Michel, H. *Structure* **1996**, *4*, 581. (c) Roszak, A. W.; Howard, T. D.; Southall, J.; Gardiner, A. T.; Law, C. J.; Isaacs, N. W.; Cogdell, R. J. *Science* **2003**, *302*, 1969.
(3) (a) Michelsen, U.; Hunter, C. A. *Angew. Chem., Int. Ed.* **2000**, *39*, 764. (b) Ikeda, C.; Satake, A.; Kobuke, Y. *Org. Lett.* **2003**, *5*, 4935. (c) Kim, D.; Osuka, A. *Acc. Chem. Res.* **2004**, *37*, 735. (d) Sprafke, J. K.; Odell, B.; Claridge, T. D. W.; Anderson, H. L. *Angew. Chem., Int. Ed.* **2011**, *50*, 5572. (e) Bhosale, R.; Misek, J.; Sakai, N.; Matile, S. *Chem. Soc. Rev.* **2010**, *39*, 138. (f) Rousseaux, S. A. L.; Gong, J. Q.; Haver, R.; Odell, B.; Claridge, T. D. W.; Herz, L. M.; Anderson, H. L. *J. Am. Chem. Soc.* **2015**, *137*, 12713. (g) Jiang, H. W.; Tanaka, T.; Kim, T.; Sung, Y. M.; Mori, H.; Kim, D.; Osuka, A. *Angew. Chem., Int. Ed.* **2015**, *54*, 15197. (h) Sung, Y. M.; Yoon, M. C.; Lim, J. M.; Rath, H.; Naoda, K.; Osuka, A.; Kim, D. *Nat. Chem.* **2015**, *7*, 418.
(4) (a) Lefler, K. M.; Brown, K. E.; Salamant, W. A.; Dyar, S. M.; Knowles, K. E.; Wasielewski, M. R. *J. Phys. Chem. A* **2013**, *117*, 10333. (b) Renaud, N.; Sherratt, P. A.; Ratner, M. A. *J. Phys. Chem. Lett.* **2013**, *4*, 1065. (c) Renaud, N.; Grozema, F. C. *J. Phys. Chem. Lett.* **2015**, *6*, 360. (d) Mallia, A. R.; Salini, P. S.; Hariharan, M. *J. Am. Chem. Soc.* **2015**, *137*, 15604.
(5) Würthner, F.; Saha-Möller, C. R.; Fimmel, B.; Ogi, S.; Leowanawat, P.; Schmidt, D. *Chem. Rev.* **2016**, *116*, 962.
(6) (a) Weil, T.; Vosch, T.; Hofkens, J.; Peneva, K.; Müllen, K. *Angew. Chem., Int. Ed.* **2010**, *49*, 9068. (b) De Schryver, F. C.; Vosch, T.; Cotlet, M.; Van der Auweraer, M.; Müllen, K.; Hofkens, J. *Acc. Chem. Res.* **2005**, *38*, 514.
(7) (a) Rybtchinski, B.; Sinks, L. E.; Wasielewski, M. R. *J. Phys. Chem. A* **2004**, *108*, 7497. (b) Veldman, D.; Chopin, S. M. A.; Meskers, S. C. J.; Groeneveld, M. M.; Williams, R. M.; Janssen, R. A. J. *J. Phys. Chem. A* **2008**, *112*, 5846. (c) Kistler, K. A.; Pochas, C. M.; Yamagata, H.; Matsika, S.; Spano, F. C. *J. Phys. Chem. B* **2012**, *116*, 77. (d) Lindquist, R. J.; Lefler, K. M.; Brown, K. E.; Dyar, S. M.; Margulies, E. A.; Young, R. M.; Wasielewski, M. R. *J. Am. Chem. Soc.* **2014**, *136*, 14912. (e) Hippius, C.; Schlosser, F.; Vysotsky, M. O.; Böhmer, V.; Würthner, F. *J. Am. Chem. Soc.* **2006**, *128*, 3870.
(8) (a) Dehm, V.; Büchner, M.; Seibt, J.; Engel, V.; Würthner, F. *Chem. Sci.* **2011**, *2*, 2094. (b) Son, M.; Fimmel, B.; Dehm, V.; Würthner, F.; Kim, D. *ChemPhysChem* **2015**, *16*, 1757. (c) Fimmel, B.; Son, M.; Sung, Y. M.; Grüne, M.; Engels, B.; Kim, D.; Würthner, F. *Chem. - Eur. J.* **2015**, *21*, 615.
(9) For general reviews on foldamers, see (a) Hecht, S., Huc, I., Eds. *Foldamers: Structure, Properties and Applications*; Wiley-VCH: Weinheim, 2007. (b) Horne, W. S.; Gellman, S. H. *Acc. Chem. Res.* **2008**, *41*, 1399. (c) Saraogi, I.; Hamilton, A. D. *Chem. Soc. Rev.* **2009**, *38*, 1726. (d) Guichard, G.; Huc, I. *Chem. Commun.* **2011**, *47*, 5933. (e) Martinek, T. A.; Fülöp, F. *Chem. Soc. Rev.* **2012**, *41*, 687.
(10) (a) Schlosser, F.; Stepanenko, V.; Würthner, F. *Chem. Commun.* **2010**, *46*, 8350. (b) Schlosser, F.; Sung, J.; Kim, P.; Kim, D.; Würthner, F. *Chem. Sci.* **2012**, *3*, 2778. (c) Wu, Y.; Young, R. M.; Frasconi, M.; Schneebeli, S. T.; Spenst, P.; Gardner, D. M.; Brown, K. E.; Würthner, F.; Stoddart, J. F.; Wasielewski, M. R. *J. Am. Chem. Soc.* **2015**, *137*, 13236.
(11) (a) Langhals, H.; Ismael, R. *Eur. J. Org. Chem.* **1998**, *1998*, 1915. (b) Feng, J.; Zhang, Y.; Zhao, C.; Li, R.; Xu, W.; Li, X.; Jiang, J. *Chem. - Eur. J.* **2008**, *14*, 7000. (c) Schlosser, F.; Moos, M.; Lambert, C.; Würthner, F. *Adv. Mater.* **2013**, *25*, 410. (d) Brown, K. E.; Salamant, W. A.; Shoer, L. E.; Young, R. M.; Wasielewski, M. R. *J. Phys. Chem. Lett.* **2014**, *5*, 2588. (e) Ryan, S. T. J.; Young, R. M.; Henkelis, J. J.; Hafezi, N.; Vermeulen, N. A.; Hennig, A.; Dale, E. J.; Wu, Y. L.; Krzyaniak, M. D.; Fox, A.; Nau, W. M.; Wasielewski, M. R.; Stoddart, J. F.; Scherman, O. A. *J. Am. Chem. Soc.* **2015**, *137* (9982), 15299. (f) Ball, M.; Fowler, B.; Li, P. P.; Joyce, L. A.; Li, F.; Liu, T. F.; Paley, D.; Zhong, Y.; Li, H. X.; Xiao, S. X.; Ng, F.; Steigerwald, M. L.; Nuckolls, C. *J. Am. Chem. Soc.* **2015**, *137*, 9982.
(12) (a) Spenst, P.; Würthner, F. *Angew. Chem., Int. Ed.* **2015**, *54*, 10165. (b) Spenst, P.; Young, R. M.; Wasielewski, M. R.; Würthner, F. *Chem. Sci.* **2016**, *7*, 5428.
(13) For general reviews on macrocycles composed of π-conjugated scaffolds, see (a) Nakamura, Y.; Aratani, N.; Osuka, A. *Chem. Soc. Rev.* **2007**, *36*, 831. (b) Tahara, K.; Tobe, Y. *Chem. Rev.* **2006**, *106*, 5274. (c) Spitler, E. L.; Johnson, C. A., II; Haley, M. M. *Chem. Rev.* **2006**, *106*, 5344. (d) Iyoda, M.; Yamakawa, J.; Rahman, M. J. *Angew. Chem., Int. Ed.* **2011**, *50*, 10522.
(14) (a) Wasielewski, M. R.; Niemczyk, M. P.; Svec, W. A.; Pewitt, E. B. *J. Am. Chem. Soc.* **1985**, *107*, 1080. (b) Giaimo, J. M.; Gusev, A. V.; Wasielewski, M. R. *J. Am. Chem. Soc.* **2002**, *124*, 8530. (c) Schuster, D. I.; Cheng, P.; Jarowski, P. D.; Guldi, D. M.; Luo, C.; Echegoyen, L.; Pyo, S.; Holzwarth, A. R.; Braslavsky, S. E.; Williams, R. M.; Klihm, G. *J. Am. Chem. Soc.* **2004**, *126*, 7257. (d) Whited, M. T.; Patel, N. M.; Roberts, S. T.; Allen, K.; Djurovich, P. I.; Bradforth, S. E.; Thompson, M. E. *Chem. Commun.* **2012**, *48*, 284.
(15) Chen, Z.; Fimmel, B.; Würthner, F. *Org. Biomol. Chem.* **2012**, *10*, 5845.
(16) (a) Seibt, J.; Marquetand, P.; Engel, V.; Chen, Z.; Dehm, V.; Würthner, F. *Chem. Phys.* **2006**, *328*, 354. (b) Seibt, J.; Winkler, T.; Renziehausen, K.; Dehm, V.; Würthner, F.; Meyer, H.-D.; Engel, V. *J. Phys. Chem. A* **2009**, *113*, 13475. (c) Kistler, K. A.; Pochas, C. M.; Yamagata, H.; Matsika, S.; Spano, F. C. *J. Phys. Chem. B* **2012**, *116*, 77. (d) Pochas, C. M.; Kistler, K. A.; Yamagata, H.; Matsika, S.; Spano, F. C. *J. Am. Chem. Soc.* **2013**, *135*, 3056. (e) Hestand, N. J.; Spano, F. C. *J. Chem. Phys.* **2015**, *143*, 244707.
(17) (a) Würthner, F. *Pure Appl. Chem.* **2006**, *78*, 2341. (b) Osswald, P.; Würthner, F. *Chem. - Eur. J.* **2007**, *13*, 7395. (c) Hippius, C.; van Stokkum, I. H. M.; Zangrando, E.; Williams, R. M.; Wykes, M.; Beljonne, D.; Würthner, F. *J. Phys. Chem. C* **2008**, *112*, 14626. (d) Xie, Z.; Würthner, F. *Org. Lett.* **2010**, *12*, 3204. (f) Schlosser, F.; Moos, M.; Lambert, C.; Würthner, F. *Adv. Mater.* **2013**, *25*, 410.
(18) Fron, E.; Schweitzer, G.; Osswald, P.; Würthner, F.; Marsal, P.; Beljonne, D.; Müllen, K.; De Schryver, F. C.; Van der Auweraer, M. *Photochem. Photobio. Sci.* **2008**, *7*, 1509.
(19) Moore, J. S.; Ray, C. R. In *Poly(arylene etynylene)s: From Synthesis to Application*; Weder, C., Ed.; Springer Berlin Heidelberg: Berlin, Heidelberg, 2005; pp 91−149.
(20) Pace, C. N.; Shirley, B. A.; Thompson, J. A. *Protein Structure: A Practical Approach*; IRL Press: New York, 1989.
(21) Brown, K. E.; Veldkamp, B. S.; Co, D. T.; Wasielewski, M. R. *J. Phys. Chem. Lett.* **2012**, *3*, 2362.
(22) Sung, J.; Nowak-Król, A.; Schlosser, F.; Fimmel, B.; Kim, W.; Kim, D.; Würthner, F. *J. Am. Chem. Soc.* **2016**, *138*, 9029.
(23) Usui, Y. *Chem. Lett.* **1973**, *2*, 743.
(24) Son, M.; Park, K. H.; Shao, C.; Würthner, F.; Kim, D. *J. Phys. Chem. Lett.* **2014**, *5*, 3601.



DOI: 10.1021/jacs.6b11973
*J. Am. Chem. Soc.* 2017, 139, 2014−2021